Spectroscopic Analysis of Amorphous Structure in Fluorinated Polymers

Yuning Yang,† Guolin Wu, Suriyakala Ramalingam,‡ and Shaw Ling Hsu*

Polymer Science and Engineering Department and Materials Research Science and Engineering Center, University of Massachusetts, Amherst, Massachusetts 01003

Lothar Kleiner and Fuh Wei Tang

Abbott Cardio Vascular, 3200 Lakeside Drive, Santa Clara, California 95054

Received July 27, 2007; Revised Manuscript Received October 23, 2007

ABSTRACT: High-quality polarized Raman spectra have been obtained for various poly(vinylidene fluoride) (PVDF) structures, crystalline and amorphous. The results encouraged us to revisit the Raman band assignment, especially within the conformational sensitive region (400−1100 cm^{-1}) and to use the new understanding to characterize the amorphous region of PVDF. Vibrational bands have been assigned on the basis of polarization characteristics observed and the potential energy distribution (PED) calculated. The simulated results agree well with the experimental polarized Raman study. On the basis of the calculated PED, combined with the simulation of different conformational sequences (*tttt*, *tttg*, *tgtg′ tggg*, *gggg*), spectroscopic features (band intensity at 648 cm^{-1} and the frequency change of the 856 cm^{-1} band) were associated with the distribution of rotational isomeric states. Two rotational isomeric state (RIS) models were analyzed and compared in the simulation of the amorphous state. On the basis of the spectroscopic features of experimental and simulated Raman spectra, it was concluded that the model which predicts higher gauche population more accurately describes the amorphous state. This analysis provides an opportunity to describe the amorphous state in a quantitative manner.

Introduction

Fluorinated polymers have a broad spectrum of applications. A well-known polymer in this family is poly(vinylidene fluoride) (PVDF). This polymer, known for its attractive piezoelectric properties, is used in a number of commercial electromechanical devices such as speakers and microphones.[1] The piezoelectric property is an inherent property of the poled crystalline phase generally obtained at elevated temperatures and in the presence of a strong electric field. Therefore, the polymorphism of the crystalline phase of PVDF has been studied in great detail.[2] Five possible crystalline phases of PVDF have been revealed, namely, α, β, γ, α_p, and ϵ, which possess different chain conformations.[3−7] The chains in the α-crystal have a *tgtg′* conformation. The β crystal, responsible for the piezo- and pyroelectric properties, has a *tttt* planar zigzag chain conformation. The γ-crystal possesses a *tttgtttg′* conformation. The two remaining phases, α_p and ϵ, are rarely observed. These different crystalline phases can be formed by varying thermal, mechanical, or electrical treatments.[8−14] It is also known that different solvents can dissolve PVDF, and the cast films from these solutions appear with different crystal forms.[15−17]

Although most PVDF studies to date have focused on the features of various crystalline phases, details of the structure associated with the amorphous phase are also of interest. PVDF, together with its copolymers, has been used as the major component in diverse applications as fluoroelastomers such as Viton or in electrolyte membranes for secondary lithium battery and fuel applications.[18] In addition, the application of PVDF as a biomedical material has also been increasing. In applications such as generation of soft tissue, suture material, and biomembranes,[19−21] PVDF is used due to its desirable biocompatibility, biostability, and satisfactory mechanical strength.[19,22−24]

The amorphous phase of PVDF has been studied by various techniques. Differential scanning calorimetry (DSC), thermostimulated current (TSC), dielectric, mechanical, and nuclear magnetic resonance (NMR) spectroscopy have been used to investigate various relaxation behavior in the amorphous phase.[25−31] The conversions between amorphous and polymorphic crystalline phases under various thermal conditions have been studied using NMR and vibrational spectroscopy.[32−34] Dilute-solution properties and unperturbed dimensions of PVDF molecules have been investigated.[35,36] The conformational characteristics of unperturbed PVDF chains in dilute solution,[37] conformational energies calculation for PVDF model compounds,[18] and molecular dynamics simulations for PVDF melts[38] have also been conducted. However, quantitative studies on the structure of PVDF amorphous chains in the condensed phase remain lacking.

In the current study, a spectroscopic method combining experimental Raman spectroscopy and a simulation method based on normal-coordinate analysis is used to obtain quantitative information on the PVDF amorphous phase in the condensed phase. Raman spectroscopy is an ideal tool to detect localized structures at the molecular scale, which is particularly useful for characterizing conformational distribution in the amorphous phase. In our previous studies, on the basis of the original algorithm first developed by Snyder and co-workers, we developed a number of techniques to characterize amorphous polymer structures in the condensed state. For polymers in solution or melt, there is a total absence of long-range order. There are few techniques that are capable of elucidating the conformational distribution for these disordered polymers. We found that isotropic Raman scattering can be used to characterize the differences in conformational distribution. Our first study

* To whom correspondence should be addressed: tel 413-577-1125; e-mail slhsu@polysci.umass.edu.
† Physics Department.
‡ Chemistry Department.

10.1021/ma071681m CCC: $37.00
Published on Web 11/22/2007

concentrated on differences in the chain statistics of poly(ethylene oxide) in solution or melt.[39] In the aqueous solution *tgt* is the dominant rotational isomeric state in the overall conformational distribution. In contrast, the dominant state in PEO melt is *tgg*.[39] Subsequently, we employed this technique to characterize disordered polymer chains in a variety of polymers, including the amorphous regions in the condensed state for polyesters.[40] In addition, the analysis was sufficiently detailed to allow analysis of changes in the conformational distribution when the polyester is deformed to form the crystalline state.[41] In the present study, a similar methodology is adopted to characterize the amorphous phase of PVDF. The Raman spectrum was successfully simulated by comparison to the experimental spectrum. Spectroscopic features (the frequency change of the 856 cm^{-1} band and the intensity at 648 cm^{-1}) were found to be extremely sensitive to the conformational distribution. These features were used to analyze the conformational distribution in the condensed phase. Our results are reported here.

Experimental Section

PVDF homopolymer was obtained from Solvay. Molecular weight and its distributions were determined by GPC using DMF as solvent and polystyrene as standard. Melting temperature, heat of fusion, and degree of crystallinity were measured by differential scanning calorimetry (DSC). The physical properties of the sample include the molecular weight $M_w = 194$K g/mol, the polydispersity index $M_w/M_n = 1.91$, the melting temperature $T_m = 177.6$ °C, and the degree of crystallinity $X_c = 63.9\%$. In this study, a value of 104.7 J/g was used for the heat of fusion of 100% α-crystalline PVDF.[42]

Acetone and *N*,*N*-dimethylacetamide (DMA) were used for preparation of solution-cast films. These solvents are of reagent grade and used without further purification. PVDF solutions of different solvents were prepared at room temperature with an initial concentration of 10 wt %. A higher temperature (~45 °C) was required to dissolve PVDF homopolymer in acetone. Films of ~20 μm thickness were cast from these solutions and spread evenly on a glass slide. Solvent evaporation at room temperature took >20 h.

Raman spectra were obtained with the use of laser confocal Raman spectrometer (Jobin Yvon HORIBA LabRam HR800 Raman microscope) in the frequency range 400−1100 cm^{-1}. Spectra resolution was maintained at 4 cm^{-1}. Laser power was ~5 mW from a He−Ne laser (632.8 nm). The incident laser was highly polarized. Polarized and depolarized spectra were obtained using a polarizer supplied by the manufacturer.

Simulation of Raman Spectra

Conformational analysis on amorphous chains has been challenging due to the fact that amorphous chains do not possess periodicity. In this study, we used the program "Disordered Chain Normal Coordinate Analysis" (DCNCA) to simulate the Raman spectrum, which is originally developed by Snyder[43,44] and modified in our laboratory. Success has been obtained for polyolefin, polyether, and polyester.[39−41,45,46] The amorphous chains are represented by an ensemble of relatively short chains generated by a statistical distribution of various rotational isomeric states. The average chain spectrum in the ensemble is used to represent the amorphous structure. A Monte Carlo method was used to generate short polymer chains on the basis of the appropriate rotational isomeric state (RIS) model. The simulation spectra are taken to be the sum of spectra of individual chains.

$$S(\upsilon) = \sum_{i=1}^{m} S_i(\upsilon) \tag{1}$$

$$S_i(\upsilon) = \sum_{j=1}^{3n-6} I(a_j, b_j, c, \upsilon) \tag{2}$$

where $S(\upsilon)$ is the isotropic Raman spectrum, $S_i(\upsilon)$ is the spectrum of the ith chain, m is the total number of chains considered, I is the band shape function, a is the intensity, b is the frequency of a mode, c is the half-width, and j is the summation variable representing each of the $3n - 6$ normal modes in a molecule with n atoms. The Raman intensities were calculated using a simple bond polarizability model.[47] For PVDF, the bond polarizability model includes contributions from seven sets of coordinates. They are backbone bond stretching C−C, backbone bond angle bending $C_H-C_F-C_H$, $C_F-C_H-C_F$, and the stretching C−F, bending F−C−C, F−C−F, C−C−H, where the subscripts H and F indicate the type of side atoms that the carbon atom is connected with. The scattering activity of the jth mode of a chain is given by

$$a_j = \left(\sum_{\alpha=1}^{7} A_\alpha \sum_k L_{kj}^{\alpha}\right)^2 \tag{3}$$

where A_α is an intensity parameter which is proportional to the derivative of the mean polarizability of the αth coordinate, and L_{kj}^{α} is the kth element in the normal coordinate associated with the αth coordinate. The values of A_α used in the present study are 1.0, 0.8, 0.1, 0.2, 0.4, 0.5, and 0.1 for C−C, C−F, F−C−C, F−C−F, $C_H-C_F-C_H$, $C_F-C_H-C_F$, and C−C−H, respectively. The force field was transferred from previous PVDF studies and has been shown to be successful for all three PVDF crystalline forms.[48] In that study, there are two sets of force fields for α and β crystalline form. In order to simulate the amorphous phase, we chose one consistent force field in our study. The force constant for the β crystalline form is sufficient for simulation of α and β crystalline forms as well as the amorphous phase. The force field adopted in this study is shown in Table 1.

The molecular structural parameters used in this study are shown below: the C−H, C−F, and C−C bonds used were 1.096, 1.34, and 1.54 Å, respectively. The F−C−F and H−C−H valence angles were taken as 109.5°. The $C_H-C_F-C_H$ was taken as 118.5° and $C_F-C_H-C_F$ as 116.5°. Torsional angles were assumed to be either trans ($t = 180°$), gauche ($g = 60°$), or gauche′ ($g' = -60°$). Since the simulation was carried on for an ensemble of short chains, the effect of the end group needs to be investigated. Therefore, simulations were carried out as a function of the number of repeat units, and the spectra are shown in Figure 1. These indicate there is some variation for extremely short chains because of the end group effects. As expected, these perturbations diminish with increasing number of repeat units. The spectra converge very well above 10 repeat units. Therefore, the number of repeat units is chosen to be 10 in this simulation study.

Results and Discussion

Normally, most of the Raman-active backbone bond stretching and skeletal bending modes of polymers fall in the frequency range of 400−1100 cm^{-1}. These modes are sensitive to the conformational change, as our previous studies have shown.[39−41,45,46] Therefore, in order to characterize the conformational distribution for PVDF, we focused on this 400−1100 cm^{-1} frequency

Table 1. Intramolecular Valence Force Constants of Poly(vinylidene fluoride)

no.	force constants	coordinates involved	common atoms	values[a]
1	K_d	CH		4.902
2	K_R	CC		4.413
3	F_{R1}	CC, CF	C	0.403
4	F_R	CC,CC	C	0.148
5	$F_{R\gamma}$	CC,CCH	CC	0.206
6	$F_{R\omega}$	CC, CCC	CC	0.273
7	$F_{R\phi}$	CC, CCF	CC	0.567
8	F_d	CH,CH	C	0.058
9	K_1	CF		5.96
10	F_{11}	CF,CF	C	0.621
11	$F_{1\xi}$	CF, CFF	CF	0.674
12	H_γ	CCH		0.615
13	F_γ	CCH,CCH	CC	0.105
14	F_γ'	CCH, CCH	CH	0.074
15	H_δ	CHH		0.441
16	H_ω	CCC		1.248
17	f_ω^t	CCC, CCC (t)	CC	−0.036
18	H_ϕ	CCF		1.262
19	H_ξ	CFF		1.50
20	T	CCCC		0.05
21	$F_{1\phi}$	CF, CCF	CF	0.62
22	F_ϕ	CCF, CCF	CC	0.178
23	F_ϕ'	CCF, CCF	CF	0.143
24	$f_{\omega\gamma}^g$	CCC, CCH (g)	CC	0.138
25	$f_{\omega\phi}^g$	CCC, CCF (g)	CC	−0.085
26	$f_{\gamma\phi}^t$	CCH, CCF (t)	CC	0.063
27	$f_{\gamma\phi}^g$	CCH, CCF (g)	CC	0.055

[a] The stretch constants have units of mdyn/Å, the stretch−bend interactions have units of mdyn/rad, and the bending constants have units of (mdyn Å)/rad^2.

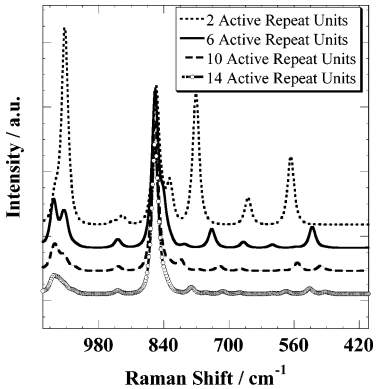

Figure 1. Simulated Raman spectra of PVDF as a function of repeat unit.

region. The simulation methodology, structure, and force field were validated by investigating experimental and simulated Raman spectra of α and β crystalline forms. A sample of the β form was prepared by casting films from *N*,*N*-dimethylacetamide (DMA) solution, and a sample of the α form was prepared by casting films from acetone solution.[48] The experimental Raman spectra of α and β forms are shown in Figure 2. Raman simulations were then carried out for α and β forms. For β forms, all torsional angles along the backbone were set to be 180°. For the α form, torsional angles were set to be repeating sequences of *tgtg′*, where $t = 180°$, $g = 60°$, and $g' = -60°$. The simulated spectra are shown in Figure 3. The agreement between experimental data and simulated spectra is excellent and provides considerable confidence in the structure and force field employed.

The strongest Raman active band is at 798 cm^{-1} and assigned to the CH_2 rocking mode and anisotropic species in previous studies.[49,50] However, polarized Raman data are now obtained. The polarized and depolarized components are shown in Figure

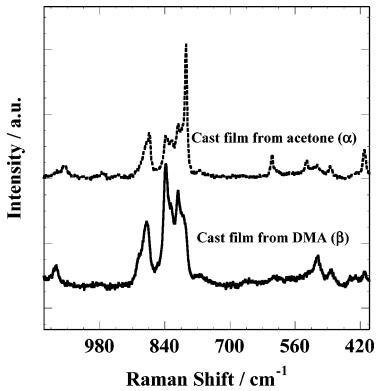

Figure 2. Experimental Raman spectra of α and β crystalline form of PVDF.

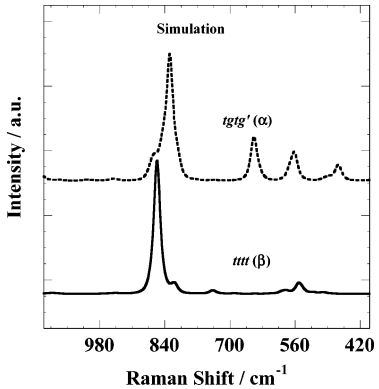

Figure 3. Simulated Raman spectra of α and β crystalline form of PVDF.

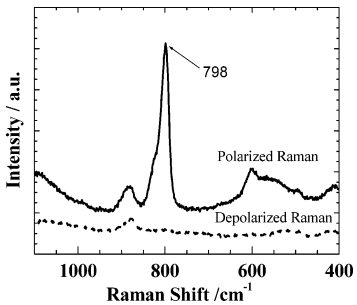

Figure 4. Polarized and depolarized experimental Raman spectra of PVDF.

4. The polarized component was obtained by setting the analyzer polarization parallel to the polarization direction of the incident beam while the depolarized component was obtained by setting the analyzer polarization perpendicular to that polarization. For the anisotropic species, there is a relationship between the depolarized and polarized component[51]

$$I_\perp = \frac{3}{4} I_{||} \tag{4}$$

where $I_\perp$ is the intensity of the depolarized component and $I_{||}$ is the intensity of the polarized component. On the other hand, for the isotropic species the depolarized component is equal to zero.[51] In Figure 4, the band intensity of the 798 cm^{-1} was zero, rather than 3/4 of intensity of the polarized component as expected. Therefore, the band at 798 cm^{-1} should belong to the isotropic species, contrary to the assignment reported in the literature. On the basis of this inconsistency determined, a more detailed analysis of Raman spectra is necessary.

Bands were also assigned on the basis of the potential energy distribution (PED) calculation. The PED is determined by the

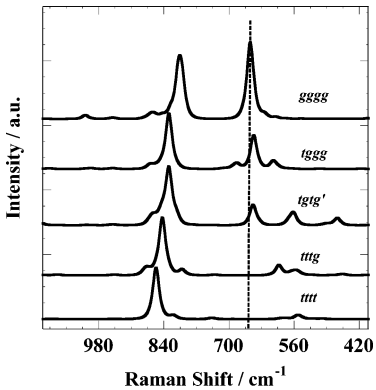

Figure 5. Simulated Raman spectra of different conformational sequences of PVDF.

contribution of each force constant f_{ij} to the normal frequencies of vibration.[52] For the ith normal frequency, the total potential energy λ_i is given by

$$\lambda_i = \sum_{jk} L_{ji} L_{ki} f_{jk} \tag{5}$$

where L_{ji} and L_{ki} are eigenvectors and f_{jk} is the force constant. The PED for the ith normal frequency and jth force constant is expressed by

$$(\mathrm{PED})_{ij} = \frac{100 L_{ji}^{\,2} f_{jj}}{\lambda_i} \tag{6}$$

Band assignment was then carried out on the basis of the character of the mode and polarization intensity measured. For the β form, two major bands appear in the simulated spectrum. The band at 856 cm^{-1} is dominated by CF stretching (51%), and the band at 550 cm^{-1} is assigned to the skeletal bending, FCF (36%) + CCF (30%). For the α form, there are five major bands. The band at 864 cm^{-1} is assigned to CCH deformation (48%). The band at 830 cm^{-1} is a combination of CC (27%) + CCC (16%). The band at 648 cm^{-1} is assigned to skeletal deformation involving CCF (34%) + CCC (13%). The 562 cm^{-1} band is assigned to skeletal bending involving FCF (40%) and CCF (32%). Last, the band at 468 cm^{-1} is assigned to CCF (53%). Because the mass difference between fluorine and carbon atoms is only ~3, the separation between stretching and other lower skeletal deformations does not exist for PVDF. Most of our assignments agree with the results in the literature. However, the band at 830 cm^{-1} which corresponds to the 798 cm^{-1} experimental band is assigned to CC and CCC, respectively. Both belong to isotropic species. This assignment is consistent with the polarized Raman spectrum obtained.

After validation of the simulation method and force field, we focused on the utility of Raman analysis to characterize the amorphous phase. First, in order to examine the effect of conformational change on the Raman spectrum, we conducted simulation on PVDF molecules with totally different conformations along the backbone. Figure 5 shows simulation results for PVDF molecules with five different conformational sequences: *tttt*, *tttg*, *tgtg′*, *tggg*, and *gggg*. Each sequence was repeated along the backbone of the molecule. It is evident that the Raman spectra are very sensitive to the conformational change. The band at 648 cm^{-1} in the *tgtg′* conformational sequence is especially sensitive to the percentage of the gauche population. This band is nonexistent in the spectra simulated for PVDF chains with *tttt* and *tttg* conformations. However, its intensity increases dramatically for chains containing *tgtg′*, *tggg*, and *gggg* conformations. On the basis of the PED calculation for the α crystalline form, this 648 cm^{-1} band is assigned to the CCF (34%) + CCC (13%) deformation band. This skeletal deformation mode should be extremely sensitive to changes in conformational distribution. As demonstrated in the simulations, the sensitivity of this 648 cm^{-1} band is a very good indicator for the conformational distribution or amount of gauche content. The band at 856 cm^{-1} is assignable to the *tttt* sequence. The frequency continues to shift downward with increasing gauche content. In the *gggg* sequence, this band is located at an extremely low frequency of 806 cm^{-1}.

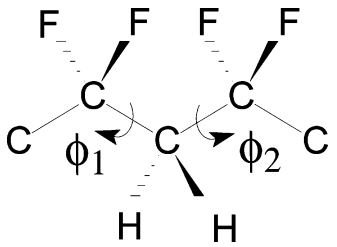

Figure 6. Geometry of torsional angles ϕ_1 (CF_2 centered) and ϕ_2 (CH_2 centered) for PVDF.

In order to simulate the amorphous phase, it is necessary to determine the probability distribution among different torsional states (t, g, g') for each torsional angle along the backbone. This probability distribution has been described by different RIS models reported in the literature. Tonelli has evaluated the RIS model for PVDF on the basis of an approximate conformational energy calculation (model A)[37] based on intramolecular electrostatic and van der Waals interactions. The geometry of torsional angles ϕ_1 (CF_2 centered) and ϕ_2 (CH_2 centered) is shown in Figure 6. The conditional probabilities matrices of torsional angles ϕ_1 and ϕ_2 of model A are

$$U_1^{\mathrm{A}} = \begin{pmatrix} 0.472 & 0.264 & 0.264 \\ 0.596 & 0.272 & 0.132 \\ 0.596 & 0.132 & 0.272 \end{pmatrix} \quad U_2^{\mathrm{A}} = \begin{pmatrix} 0.264 & 0.368 & 0.368 \\ 0.324 & 0.382 & 0.294 \\ 0.324 & 0.294 & 0.382 \end{pmatrix}$$

Using this RIS model, the overall gauche population at a temperature of 463 K is 51%. On the other hand, Byutner proposed a different RIS model for PVDF in 1999 (model B).[18] The model is derived from high-level quantum chemistry calculations for several PVDF model compounds. The probabilities matrices calculated from model B are

$$U_1^{\mathrm{B}} = \begin{pmatrix} 0.168 & 0.416 & 0.416 \\ 0.439 & 0.518 & 0.043 \\ 0.439 & 0.043 & 0.518 \end{pmatrix} \quad U_2^{\mathrm{B}} = \begin{pmatrix} 0.052 & 0.474 & 0.474 \\ 0.502 & 0.462 & 0.036 \\ 0.502 & 0.036 & 0.462 \end{pmatrix}$$

In Byutner's model, the trans state can be split into two states: $t_+ = 195°$ and $t_- = 165°$. In our calculation, these two states are merged into one trans state $t = 180°$. The gauche population was calculated to be 65% at temperature 463 K, which is much higher than the percentage as reported in model A (51%).

Raman simulations of the amorphous state were carried out on the basis of both models. The experimental Raman spectrum of PVDF in the molten state was also obtained. Figure 7 presents experimental spectra of the α, β crystalline form and molten state. The most dominant band in the α form is at 794 cm^{-1}, while in the β form it is at 838 cm^{-1}. In the molten state, the dominant band is also at 794 cm^{-1}, which is at the same position as the dominant band in the α form. In the α form, the conformational sequence is *tgtg′*, while in the β form the sequence is *tttt*. Therefore, the fact that this dominant band is

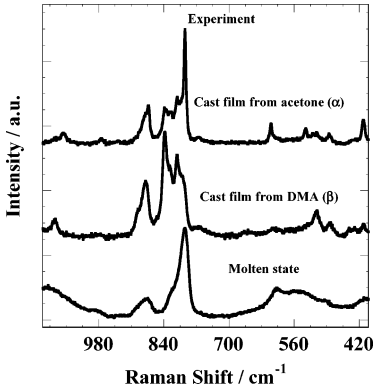

Figure 7. Experimental Raman spectra of PVDF in molten state and in α and β crystalline form.

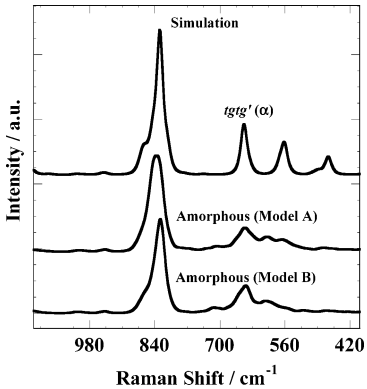

Figure 8. Simulated Raman spectra of amorphous phase based on rotational isomeric model A (Tonelli's) and model B (Byutner's) and simulated spectrum of α crystalline form of PVDF.

found at the same position between the molten state and α form is suggestive of a high gauche content in the amorphous state.

Another noticeable spectroscopic feature is the band intensity at 610 cm^{-1}. This band intensity normalized to the dominant component is very weak in the β form, much stronger in the α form, and even stronger in the amorphous state. According to our previous simulations of different conformational sequences, this band (648 cm^{-1} in simulation) is assigned to backbone bending modes CCF and CCC, and its intensity increases with increasing gauche population. The normalized intensities of the 610 cm^{-1} band are equal to 0.16 and 0.31 for the α form and amorphous state, respectively. Since the gauche population in the α form is 50%, this result from experimental spectra suggests the gauche population in the amorphous state is even higher than 50%. The simulated Raman spectra based on models A and B are shown in Figure 8 together with the simulated spectrum of the α form. The dominant band in the α form spectrum and amorphous spectrum from model B are both at 828 cm^{-1}, while the dominant band is at 838 cm^{-1} in the amorphous spectrum deduced from model A. In the experimental spectra, the dominant band in the α form has the same frequency as in the molten state. Therefore, simulation based on model B better fits the experimental result and predicts the consistency of position of the dominant band in both the α form and amorphous state. The normalized band intensities near 648 cm^{-1} are 0.30 and 0.24 for model B and model A, respectively. Compared to the experimental value 0.31, it is evident that model B much better agrees with experimental results. Therefore, both the frequency of the 828 cm^{-1} band and the intensity of the 648 cm^{-1} band provide support that model B (Byutner's) describes the amorphous state better in comparison to model A. It was concluded that our Raman simulation of the amorphous state is successful and the RIS model, predicting higher gauche population, accurately describes the amorphous state. These spectroscopic features allow the possibility for a quantitative analysis of amorphous structure in the condensed state. We will utilize this result in an upcoming paper in which amorphous PVDF chains in solution state in different solvents will be analyzed by this spectroscopic method and thus explain solvent-induced polymorphism in PVDF.

Conclusions

Experimental and simulated Raman spectra have been obtained for PVDF α and β crystalline forms. The combination of experiment and simulation analyses has proven valuable in assigning Raman active vibrations and to determine the conformational distribution of amorphous PVDF chains. The molecular structure and force fields used in the simulation were validated on the basis of results obtained for the crystalline phases and associated chain conformations. The potential energy distribution of Raman bands within the conformational sensitive region (400−1100 cm^{-1}) was calculated. Simulation results of different conformational sequences, combined with the calculated PED, provide spectroscopic features (the shifting of the 856 cm^{-1} band and the band intensity at 648 cm^{-1}) characterizing the distribution of conformational states. An experimental Raman spectrum was obtained for PVDF in the amorphous state. Raman simulation of the amorphous state was also carried out on the basis of two different RIS models. The simulation proved successful by comparison to the experimental spectrum. By utilizing the spectroscopic features revealed in previous results and comparison to the experimental Raman spectrum, it was concluded that the model which predicts a higher gauche population (61%) accurately describes the amorphous state.

Acknowledgment. This research has been funded by a grant from the National Science Foundation Materials Research Science and Engineering Center at University of Massachusetts and one from Abbott Cardio Vascular.

References and Notes

(1) Nalwa, H. In *Ferroelectric Polymers*; M. Dekker: New York, 1995.
(2) Lovinger, A. J. In *Developments in Crystalline Polymer*; Bassett, D. C., Ed.; Springer: Berlin, 1982.
(3) Lovinger, A. J. *Macromolecules* **1983**, *16*, 1529.
(4) Giannetti, E. *Polym. Int.* **2001**, *50*, 10.
(5) Broadhust, M. G.; Davis, G. T.; DeReggi, A. S.; Roth, S. C.; Collins, R. E. *Polymer* **1982**, *23*, 22.
(6) Tazaki, M.; Wada, R.; Okabe, M.; Homma, T. *J. Appl. Polym. Sci.* **1997**, *65*, 1517.
(7) Lee, W.-K.; Ha, C.-S. *Polymer* **1998**, *39*, 7131.
(8) Scheinbeim, J. I.; Newman, B. A.; Sen, A. *Macromolecules* **1986**, *19*, 1454.
(9) Davies, G. R.; Singh, H. *Polymer* **1979**, *20*, 772.
(10) Sajkiewicz, P. *J. Polym. Sci., Part B: Polym. Phys.* **1994**, *32*, 313.
(11) Lu, F. J.; Hsu, S. L. *Macromolecules* **1986**, *19*, 326.
(12) EI Mohajir, B.-E.; Heymans, N. *Polymer* **2001**, *42*, 5661.
(13) Weinhold, S.; Litt, M. H.; Lando, J. B. *Macromolecules* **1980**, *13*, 1178.
(14) Hsu, C. C.; Geil, P. H. *J. Appl. Phys.* **1984**, *56*, 2404.
(15) Benz, M.; Euler, W. B.; Gregory, O. J. *Macromolecules* **2002**, *35*, 2682.
(16) Grecorio, R.; Cestari, M. *J. Polym. Sci., Part B: Polym. Phys.* **1994**, *32*, 858.
(17) Salimi, A.; Yousefi, A. A. *J. Polym. Sci., Part B: Polym. Phys.* **2004**, *42*, 3487.
(18) Byutner, O. G.; Smith, G. D. *Macromolecules* **1999**, *32*, 8376.
(19) Laroche, G.; Marois, Y.; Guidoin, R.; King, M. W.; Martin, L.; How, T.; Douville, Y. *J. Biomed. Mater. Res.* **1995**, *29*, 1525.
(20) Mary, C.; Marois, Y.; King, M. W.; Laroche, G.; Douville, Y.; Martin, L.; Guidoin, R. *ASAIO J.* **1998**, *44*, 199.
(21) Bouaziz, A.; Richert, A.; Caprani, A. *Biomaterials* **1997**, *18*, 107.

(22) Liu, T. Y.; Lin, W. C.; Huang, L. Y.; Chen, S. Y.; Yang, M. C. *Polym. Adv. Technol.* **2005**, *16*, 413.
(23) Klinge, U.; Klosterhalfen, B.; Ottinger, A. P.; Junge, K.; Schumpelick, V. *Biomaterials* **2002**, *23*, 3487.
(24) Urban, E.; King, M. W.; Guidoin, R. *ASAIO J.* **1994**, *40*, 145.
(25) Teyssedre, G.; Bernes, A.; Lacabanne, C. *J. Polym. Sci., Part B: Polym. Phys.* **1993**, *31*, 2027.
(26) Wentink, T. *J. Appl. Phys.* **1961**, *32*, 1063.
(27) Ishida, Y.; Watanabe, M.; Yamafuji, K. *Kolloid Z. Z. Polym.* **1964**, *200*, 48.
(28) Kakutani, H. *J. Polym. Sci., Part A-2* **1970**, *8*, 1177.
(29) Lando, J. B.; Olf, H. G.; Peterlin, A. *J. Polym. Sci., Part A-1* **1966**, *4*, 941.
(30) Sasabe, H.; Saito, S.; Asahina, M.; Kakutani, H. *J. Polym. Sci., Part A-2* **1969**, *7*, 1405.
(31) Slichter, W. P. *J. Polym. Sci.* **1957**, *24*, 173.
(32) Holstein, P.; Harris, R. K.; Say, B. *J. Solid State Nucl. Magn. Reson.* **1997**, *8*, 201.
(33) Holstein, P.; Scheler, U.; Harris, R. K. *Polymer* **1998**, *39*, 4937.
(34) Peng, Y.; Wu, P. Y. *Polymer* **2004**, *45*, 5295.
(35) Welch, G. J. *Polymer* **1974**, *15*, 429.
(36) Ali, S.; Raina, A. K. *Makromol. Chem.* **1978**, *179*, 2925.
(37) Tonelli, A. E. *Macromolecules* **1976**, *9*, 547.
(38) Byutner, O. G.; Smith, G. D. *Macromolecules* **2000**, *33*, 4264.
(39) Yang, X.; Su, Z.; Wu, D.; Hsu, S. L.; Stidham, H. D. *Macromolecules* **1997**, *30*, 3796.
(40) Yang, X.; Kang, S.; Hsu, S. L.; Stidham, H. D.; Smith, P. B.; Leugers, A. *Macromolecules* **2001**, *34*, 5037.
(41) Yang, X.; Kang, S.; Yang, Y.; Aou, K.; Hsu, S. L. *Polymer* **2004**, *45*, 4241.
(42) Nakagawa, K.; Ishida, Y. *J. Polym. Sci., Part B: Polym. Phys.* **1973**, *11*, 2153.
(43) Cates, D. A.; Strauss, H. L.; Snyder, R. G. *J. Phys. Chem.* **1994**, *98*, 4482.
(44) Hallmark, V. M.; Bohan, S. P.; Strauss, H. L.; Snyder, R. G. *Macromolecules* **1991**, *24*, 4025.
(45) Hsu, S. L.; Hahn, T.; Suen, W.; Kang, S.; Stidham, H. D.; Siedle, A. R. *Macromolecules* **2001**, *34*, 3376.
(46) Hahn, T.; Suen, W.; Kang, S.; Hsu, S. L.; Stidham, H. D.; Siedle, A. R. *Polymer* **2001**, *42*, 5813.
(47) Snyder, R. G.; Kim, Y. *J. Phys. Chem.* **1991**, *95*, 602.
(48) Kobayashi, M.; Tashiro, K.; Tadokoro, H. *Macromolecules* **1975**, *8*, 158.
(49) Boerio, F. J.; Koenig, J. L. *J. Polym. Sci., Part A-2* **1971**, *9*, 1517.
(50) Bachmann, M. A.; Koenig, J. L. *J. Chem. Phys.* **1981**, *74*, 5896.
(51) Wilson, E. B., Jr.; Decius, J. C.; Cross, P. C. *Molecular Vibrations: The Theory of Infrared and Raman Vibrational Spectra;* Dover Publications: New York, 1955.
(52) Painter, P.; Coleman, M.; Koenig, J. L. *The Theory of Vibrational Spectroscopy and Its Application to Polymeric Materials*; John Wiley and Sons: New York, 1982.

MA071681M